Structured Elastomeric Submillimeter Films Displaying Magneto and Piezo Resistivity

Mariano M. Ruiz,[1] M. Claudia Marchi,[2] Oscar E. Perez,[3] Guillermo E. Jorge,[4†] Mirta Fascio,[5] Norma D'Accorso,[5] R. Martín Negri[1]

[1]Instituto de Química Física de Materiales, Ambiente y Energía (INQUIMAE, CONICET-UBA), Departamento de Química Inorgánica, Analítica y Química Física, Facultad de Ciencias Exactas y Naturales, Universidad de Buenos Aires, Buenos Aires, Argentina
[2]Centro de Microscopías Avanzadas (CMA) and Departamento de Química Inorgánica, Analítica y Química Física, Facultad de Ciencias Exactas y Naturales, Universidad de Buenos Aires, Buenos Aires, Argentina
[3]Departamento de Industrias, Facultad de Ciencias Exactas y Naturales, Universidad de Buenos Aires, Buenos Aires, Argentina
[4]Instituto de Ciencias, Universidad Nacional de General Sarmiento, Buenos Aires, Argentina
[5]Centro de Investigación en Hidratos de Carbono (CIHIDECAR, CONICET-UBA), Departamento de Química Orgánica, Facultad de Ciencias Exactas y Naturales, Universidad de Buenos Aires, Buenos Aires, Argentina
Correspondence to: N. D'Accorso (E-mail: norma@qo.fcen.uba.ar) or R. M. Negri (E-mail: rmn@qi.fcen.uba.ar)

Received 17 November 2014; revised 29 December 2014; accepted 6 January 2015; published online 00 Month 2015
DOI: 10.1002/polb.23672

ABSTRACT: Structured elastomer films (100–150 μm) presenting piezo and magneto resistance are described. The films are composites of filler particles, which are both electrically conductive and magnetic, dispersed in an elastomeric matrix. The particles consist of magnetite (6 nm) grouped in silver-coated aggregates (Fe_3O_4@Ag). The matrix is styrene–butadiene rubber (SBR) in which diethylene glycol (DEG) is added. The particles, SBR and DEG, are dispersed in toluene and then placed between two rare earth magnets. Formation of pseudo-chains (needles) of inorganic material aligned in the direction of the magnetic field is obtained after solvent evaporation. The addition of DEG is substantial to obtain an electrically conductive material. The electrical conductivity is anisotropic and increases when applying normal stresses and/or magnetic fields in the direction of the needles. The elastomers, particles, and needless were characterized by XRD, SEM, EDS, FTIR, DSC, TGA, VSM, profilometry, and stress–strain analysis. © 2015 Wiley Periodicals, Inc. J. Polym. Sci., Part B: Polym. Phys. **2015**, *00*, 000–000

KEYWORDS: composites; elastomers; magnetoresistive composites; piezoresistive elastomers; sensors; structured elastomers

INTRODUCTION Structured elastomer composites with anisotropic properties, such as magneto and piezoresistivity, are becoming of great interest for their potential applications in physical sensors, flexible devices, and electronic connectors.[1–9] In addition to common challenges for technological application of smart materials (obtaining appropriated quality parameters), there are specific difficulties in the case of structured elastomeric composites: (i) to develop ohmic contacts with good adherence to the elastomer; (ii) to obtain a reversible response (dependent on the elastic behavior); and (iii) to prepare submillimeter films displaying the physical properties of interest. The first two issues (contacts and reversibility) have been addressed in previous works of our group, using magnetorheological elastomers based on dispersions of magnetic nanomaterials in polydimethylsiloxane (PDMS), cured in the presence of a uniform magnetic field.[7,10] With this method it is possible to obtain structured materials formed by aligned pseudo-chains (referred to also as needles) of the fillers inside the elastomeric matrix, presenting anisotropic physical properties. We have studied, in previous works, the magnetic, electric, elastic, and morphological properties of these kinds of composites, using several different nanomaterials as fillers.[7,10–14] Those works are based on PDMS as the elastomeric matrix and were performed using slices of several millimeters thickness. The slices can be mechanically or chemically treated on its surfaces to obtain electrical conductivity through the material and to generate arrays of ohmic electrical contacts. However, to obtain anisotropic films of submillimeter thickness presenting magneto and/or piezo resistivity remains a challenge. As

†On leave from Laboratorio de Bajas Temperaturas, Universidad de Buenos Aires, Buenos Aires, Argentina.

Additional Supporting Information may be found in the online version of this article.

introducing electrically conductive filler particles creates the electrical conduction, then there is no need for using intrinsically conductive polymers, extending the possibilities for choosing the matrix according to the desired application.

Thus, the aim of this article is to report some steps toward the development of submillimeter structured elastomeric composites displaying anisotropic magneto and piezo resistivity. These objectives require not only changes in the chemical aspects related to preparation of composites but also of the physical features associated with generating structured films. In particular, PDMS is not used here but replaced by a styrene–butadiene rubber (SBR)-based polymer to build up the submillimeter elastomeric film, which can present electrical conductivity. Also the magnetic nanoparticles (magnetite, Fe_3O_4, average size <10 nm) are smaller than previously prepared, in order to ensure superparamagnetism at room temperature and to prevent, as much as possible, large irreversible magnetic effects. These nanoparticles (NPs) form agglomerates which are covered with silver (Ag^0), generating microparticles (μPs) which are simultaneously superparamagnetic and electrically conductive used as fillers in the elastomeric matrix (referred as Fe_3O_4@Ag).[7,10,11] The specific objectives of this work are to design the appropriated polymeric matrix, generate structured submillimeter composite films, and explore their piezo and magneto resistivity characteristics.

EXPERIMENTAL

Materials and Methods

Chemicals

Iron(III) chloride hexahydrate ($FeCl_3{\cdot}6H_2O$) and iron(II) chloride tetrahydrate ($FeCl_2{\cdot}4H_2O$) were purchased from Sigma-Aldrich. Sodium hydroxide (NaOH), silver nitrate ($AgNO_3$), hydrochloric acid (HCl), ammonium hydroxide (NH_4OH), tetrahydrofuran (THF), toluene, glucose monohydrate, and diethylene glycol (DEG) were all of analytical grade and used without further purification. Commercial styrene–butadiene rubber, referred as SBR, was kindly provided by Dr. Angel Marzocca from FATE S.A.I.C.I. (Argentina). Gel permeation chromatography (SEC) analysis led to a M_w of 390,000. Its composition was calculated by ^{1}H NMR, obtaining a styrene:-butadiene ratio of 23.5:76.5 with 2% w/w of carboxylated additive.

Synthesis of Magnetite Nanoparticles (Fe_3O_4 NPs)

Fe_3O_4 NPs were synthesized by the co-precipitation method. The synthesis protocol was adapted from a previous work.[11] An acidic solution (30 mL) was prepared dissolving $FeCl_3{\cdot}6H_2O$ (10^{-3} mol) and $FeCl_2{\cdot}4H_2O$ (5×10^{-4} mol) in distilled water and concentrated HCl was added to reach a final concentration of 0.4 M. The solution containing the metals was slowly added to 200 mL of a 1.5 M NaOH solution at high speed stirring previously purged by bubbling nitrogen. The synthesis temperature (60 °C) was controlled with a water-jacketed reaction vessel. After addition of the acidic solution, the precipitated particles were aged for 2 h at 60 °C. Finally, the particles were decanted by centrifugation at 20,000 *g* (10 min) and washed with distilled water. This cycle was repeated four times, and then particles were dried in a vacuum oven at room temperature for 24 h.

Synthesis of Micrometric Agglomerated of Magnetite Covered with Silver (Fe_3O_4@Ag μPs)

The preparation protocol was adapted from previous work.[11] The previously synthesized Fe_3O_4 NPs were suspended in distilled water and $AgNO_3$ was added (molar ratio Ag/Fe_3O_4 = 10:1) in ammoniacal solution as Tollens reactant. The solution containing the NPs and $Ag(NH_3)_2^+$ ion was sonicated for 30 min and then transferred to a water-jacketed reaction vessel at 50 °C. A solution containing a stoichiometric ratio of glucose monohydrate was slowly added under mechanical stirring. As the glucose was added, the solution turned brownish. The newly formed particles were decanted by centrifugation, washed, and dried exactly as described for the Fe_3O_4 NPs in the previous section.

The obtained particles, referred to as Fe_3O_4@Ag, are actually formed by μPs whose internal structure consists of several Fe_3O_4 NP clusters covered by metallic silver grouped together.

Preparation of SBR-DEG-Fe_3O_4@Ag Structured Films

Different mixtures of SBR-DEG-Fe_3O_4@Ag were prepared. A primary mixture of Fe_3O_4@Ag μPs and SBR was prepared obtaining a total weight of 0.5 g. The proportions of Fe_3O_4@Ag μPs used in this initial mixture were 5, 15, and 30% w/w. Then toluene (25 mL) was added to dissolve completely the system, which was homogenized with mechanical stirring. Different volumes (50, 100, or 200 μL) of DEG were added to this primary mixture in the different assays. Then toluene was left to evaporate (partially) under stirring at room temperature and atmospheric pressure until the system became very viscous. Afterward, the mixture was spread drop-by-drop into a cylindrical aluminum substrate (total volume added was ~1.6 mL), which was placed between two rare earth permanent magnets (disk shaped, flat surfaces, 36 mm diameter). The system was left between the magnetos at room temperature until toluene was completely evaporated to generate pseudo-chains (formed by grouping Fe_3O_4@Ag μPs), which are aligned in the direction of the magnetic field. The magnetic field between the two magnetos, close to the surface of the film and at its center, was measured with a Hall-probe (Allegro Probe Model 1302A) sensor and estimated about 800G.

Although films with different amounts of DEG were prepared at the beginning of the studies, the results presented in this work correspond to films having 18% w/w of DEG in its final composition (after complete evaporation of toluene), which correspond to an addition of 100 μL DEG into a system of 0.5 g, which contains SBR and Fe_3O_4@Ag μPs. This system is referred as SBR-DEG-% w/w Fe_3O_4@Ag structured composite, where the proportion of Fe_3O_4@Ag can change while the proportion of DEG is fixed in 18% w/w. The percentages of filler (Fe_3O_4@Ag μPs) used in the structured

films are 25, 12, and 4% w/w (these values are computed considering the addition of DEG). The word "structured" refers to films where toluene was evaporated in the presence of magnetic field which formation of pseudo-chains (needles) aligned in the direction of the magnetic and formed by grouping Fe_3O_4@Ag μPs.

Instrumentation

X-ray powder diffraction (XRD) analysis was performed with a Philips X-Pert diffractometer using Cu Kα radiation ($\lambda = 0.154056$ nm) and the average size of the Fe_3O_4 crystallites was determined by the Debye–Scherrer equation. The size distribution and morphology of the Fe_3O_4 NPs and Fe_3O_4@Ag μPs were studied using a scanning electron microscope (SEM) fitted with a field-emission source (FESEM Zeiss Supra 40 Gemini) coupled to an energy dispersive spectroscopy (EDS) detector (Oxford Instruments, model INCAx-Sight; detection limit: 0.1% w/w).

Fourier transform infrared (FTIR) analyses were performed with an FTIR Nicolet 8700 spectrometer using Smart Orbit ATR diamond crystal accessory. The baseline was corrected and normalized to the 1375 cm^{-1} peak height (polystyrene, PS, peak). Molecular weight distributions were measured by size-exclusion chromatography (SEC) using a Styragel column (HR-4) from Waters, with THF as solvent at a flow rate of 1.0 mL min^{-1}. Number and weight-average molecular weights were calculated using a universal calibration method with PS standards. Thermal analyses were performed at a heating rate of 5 K min^{-1} under nitrogen atmosphere with a differential scanning calorimetry (DSC) device DSC-TA Instrument Q-20 calibrated with indium. Exothermic reactions were measured on the first heating scan, while glass transition temperatures (T_g) were determined from subsequent heating scans. Thermal gravimetric analysis (TGA) was performed in a TGA-DTA DTG-60 Shimadzu instrument. The samples were heated from room temperature to 700 °C at 5 °C min^{-1} rate. Temperature scanning was performed under a nitrogen flux (30 mL min^{-1}), although the system is not perfectly sealed but allows the presence of oxygen. In this procedure the thermal degradation of the polymer matrix was reached at about 400 °C.

The thicknesses of the different films in the absence of external stress were measured using a surface profilometer (Veeco, model Dektak 150). Samples are placed on a glass microscope slide. The stage moves the sample beneath a diamond-tipped stylus, scanning the sample at a programmed scanning rate (12, 20, or 33 μm s^{-1} were used). The stylus is linked to a Linear Variable Differential Transformer (LDVT), which produces and processes electrical signals that correspond to surface variations of the sample. The measurements were performed in different regions of the films, scanning the samples until reaching its edge. In this way, the thickness of the film, L, was measured as function of the scanned distance. A typical range for the total distance scanned by the probe was 2000 μm. This range included scanning a broad region of the glass substrate (500–750 μm) in order to define a reference flat baseline. Average values of L, referred to as $<L>$, were calculated within defined scanning distance ranges (of 250–800 μm width depending on the sample) starting from at least 100 μm from the edge of the film.

A LakeShore 7400 Vibrating Sample Magnetometer (VSM) was used for recording magnetization curves at room temperature. In the case of Fe_3O_4 and Fe_3O_4@Ag powders, a weighted mass of the powders (5–20 mg) was packed with Teflon tape and mounted in the VSM sample holder. In the case of SBR-DEG-Fe_3O_4@Ag structured composites, a weighted cut of the film was placed in the VSM sample holder. In all cases, the magnetization curves were taken from positive saturation at 1 T, in steps of 25 mT or less, with an integration constant of 10 s for each applied magnetic field.

Stress–strain curves were registered with a Stable Microsystems TA-XT2i Texture Analyzer which compresses the sample at a constant compression speed (100 μm s^{-1}) in the range between 8 and 40% of the initial thickness, while recording the normal stress, Σ, perpendicular to the surface of the film (expressed in kPa).[15,16] These studies were conducted using SBR-DEG and SBR-DEG samples with thickness between 2 and 5 mm, that is, thicknesses that are larger than those of the structured composite films (because measurements with the texture analyzer are limited to samples of thickness >1 mm). The objective in this case was to estimate the Young's modulus of the elastomer matrix, E_m, and its elastic behavior. Different compression–decompression cycles were performed at least in duplicate to characterize the material recovery, possible ruptures, and elastic hysteresis.

The variation of electrical current (I) through the SBR-DEG-Fe_3O_4@Ag films at a fixed voltage (V_0) was measured as function of the applied normal stress, Σ. These measurements were performed by placing the films between two disk-shaped metallic electrodes. The electrodes were inserted into respective Delring™ holders to ensure rigidity. This system was vertically placed on a mechanical balance used to register the mechanical force exerted on the system, which was applied on the top electrode using a specially designed system. The voltage V_0 was applied between the electrodes using a dc-regulated voltage source, which allows changing V_0 between 100 mV and 30 V (measured with a high impedance digital tester). The current I was continuously measured while exerting the stress using another digital tester in a series circuit. When stress was changed to some value Σ while keeping V_0 fixed, then the current varied until reaching a steady-state value which is actually the reported one, I, at the stress Σ and voltage V_0. Additionally, the I–V_0 characteristic curves were obtained at a fixed Σ in order to determine the voltage range for the Ohm's law to apply. These experiments were repeated (as an additional control) using a potentiostat (TEQ-4, Argentina) varying the voltage between −1 and +1 V at a scanning rate of 100 mV s^{-1}.

In order to measure magnetoresistance effects, the device described above was placed between the pole pieces of a standard Varian low impedance electromagnet (model V3703) provided with a set of pole pieces with a diameter of 10 cm. These kinds of electromagnets are known to provide highly homogeneous steady magnetic fields, H (expressed in Oe). This magnetic field was measured with a gaussmeter (Group3 DTM-133 Digital Teslameter). I–V characteristic curves were recorded using the TEQ-4 potentiostat scanning between −100 and +100 mV (scanning rate 100 mV s^{-1}). Measurements were performed at a constant stress Σ and as function of H. The system was left to stabilize for at least 5 min previous to each determination after changing the value of the magnetic field.

RESULTS AND DISCUSSION

Characterization of the Fe_3O_4 NPs and Fe_3O_4@Ag μPs

The particle size histograms of Fe_3O_4 NPs were obtained by analyzing several SEM images and counting 300 particles in each image, approximately. One representative size histogram and the respective SEM image are shown in Supporting Information Figure SM1. The size histograms are well fitted by a lognormal distribution, with typical average size about (6.1 ± 0.1) nm and standard deviation about (0.93 ± 0.05) nm (these values remain almost independent of the considered SEM image when counting more than about 300 particles in each image while keeping the instrumental factors constant).

The XRD patterns are shown in Figure 1(a). The pattern obtained for the Fe_3O_4 NPs is in concordance with an inverse spinel structure with an average crystallite size of (5.83 ± 0.01) nm and a lattice parameter of (8.38 ± 0.01) Å, determined by Debye–Scherrer equation. The average crystallite size (5.83 nm) is in excellent agreement with the average size determined from the histogram of size distributions (6.1 nm). The experimental results indicate that the obtained Fe_3O_4 NPs constitute single-crystalline domains with a size about 6 nm, which is about half those obtained in a previous work (13 nm).[7,10,11] The reason smaller particles are obtained is the higher stirring speed used in the NaOH solution while adding the solution containing both Fe(III) and Fe(II) salts, as it has been reported that at high stirring the obtained particles tend to be smaller.[17]

In the case of Fe_3O_4@Ag, the XRD patterns show the peaks corresponding to the *fcc* structure of the Ag exclusively (those corresponding to Fe_3O_4 phase are not present) indicating that the Fe_3O_4 NPs are completely covered by Ag and not close to the μPs surface.

The magnetization curves at (25 ± 2) °C for Fe_3O_4 NPs (powder), Fe_3O_4@Ag μPs (powder), and SBR-DEG-Fe_3O_4@Ag structured films are shown in Figure 1(b). No hysteresis is observed, indicating that the three systems are in a superparamagnetic regime at room temperature. The superparamagnetic behavior is not unexpected as the Fe_3O_4 NPs are relatively small (6 nm). However, it is remarkable that the superparamagnetic behavior at 25 °C is conserved in the Fe_3O_4@Ag μPs and hence in the SBR-DEG-Fe_3O_4@Ag structured films. This indicates that the size of the Fe_3O_4 NPs is

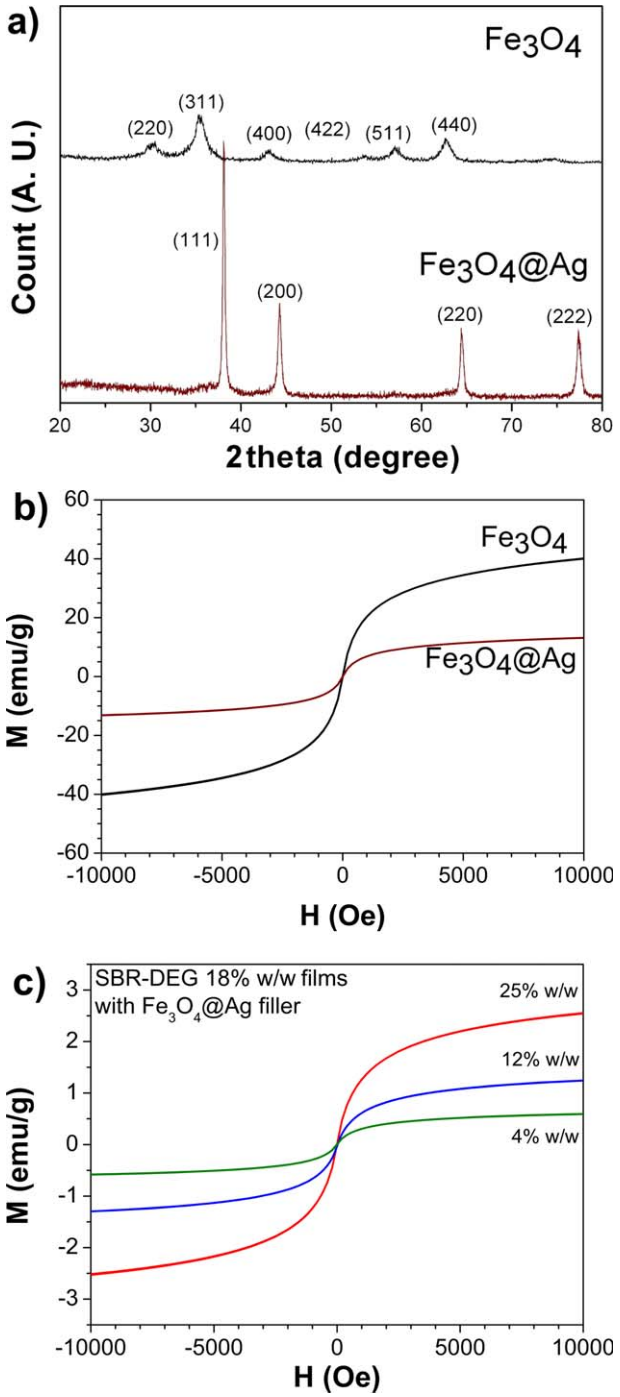

FIGURE 1 (a) XRD patterns for Fe_3O_4 NPs powder (up) and Fe_3O_4@Ag μPs powder (down). (b) Magnetization curves at room temperature for powders of Fe_3O_4 NPs and Fe_3O_4@Ag μPs. (c) Magnetization curves of SBR-DEG-Fe_3O_4@Ag composite films with three proportions of Fe_3O_4@Ag. The proportion of DEG is 18% w/w in the three cases. [Color figure can be viewed in the online issue, which is available at wileyonlinelibrary.com.]

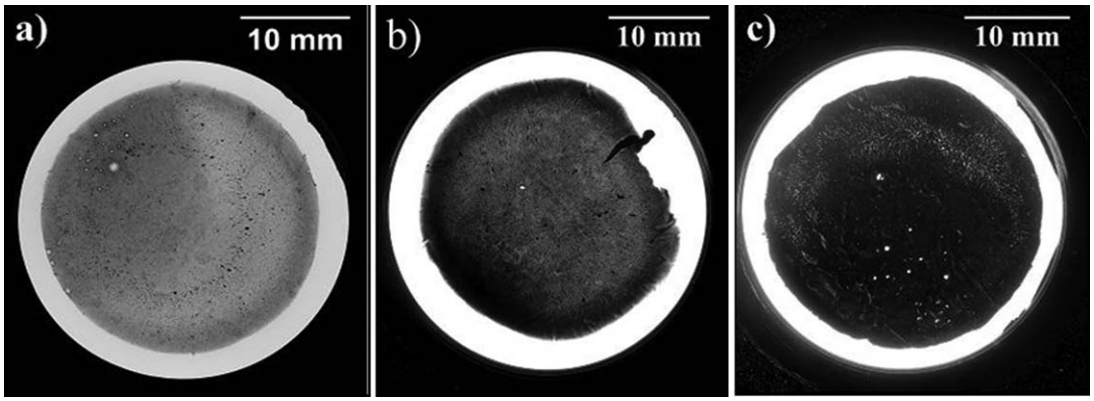

FIGURE 2 Top view pictures of composite structured films. The percentage of DEG is 18% w/w. Fe_3O_4@Ag μPs varies: (a) 4%, (b) 12%, and (c) 25% w/w, respectively.

small enough to prevent cooperative effects inside the agglomerates. And it suggests that interactions between particles inside the agglomerates cannot effectively compete with thermal disorder for establishing a magnetic order at 25 °C when the average size of the individual particles that constitute the agglomerated is below some critical value.[18,19]

At a magnetic field of 10 kOe the magnetization curves are close to reaching the magnetization of saturation, M_s. The estimated values of M_s are ≅44.1 emu g^{-1} for Fe_3O_4 NPs and ≅14.4 emu g^{-1} for Fe_3O_4@Ag μPs. From these values a silver proportion of 67% w/w is estimated in the Fe_3O_4@Ag powder.

The magnetization curves for the composite films were measured in two ways: applying the magnetic field H of the VSM device parallel and perpendicular to the orientation of formed needles in the films. In previous works we observed for micrometric PDMS-NPs slices that the value for M_s with H parallel to the needles ($M_{s//}$) always resulted higher than the value of M_s obtained applying H perpendicular to the needles ($M_{s\perp}$).[11–13] That tendency was not observed in this work probably due to experimental difficulties for aligning the thin elastic samples in the magnetometer, thus M_s values, averaged between both directions, // and ⊥, are presented in Figure 1(c).

The ratio between the values of M_s in the composite and in the Fe_3O_4@Ag powder allows obtaining a crude estimation of the filler proportion in the films if interactions between particles in the needles and magnetic and morphologic anisotropy effects are neglected. The values calculated in that manner are systematically lower than the nominal values (obtained by weighing): 19, 9, and 4% w/w (calculated using the ratio of M_s's values) for samples with 25, 12, and 4% w/w (weighted), respectively. These values are in good agreement considering the mentioned assumptions.

Morphological Characterization of SBR-DEG-Fe_3O_4@Ag Structured Films

Although mixtures with different amounts of DEG were prepared, the presented results refer to films with 18% w/w of DEG only (100 μL of DEG added to 0.5 g of the primary SBR-Fe_3O_4@Ag mixture). We observed that systems with 10% w/w of DEG (50 μL added to 0.5 g) are not electrically conductive, while the mixture SBR-DEG with 31% w/w of DEG (200 μL added to 0.5 g) is not miscible (independently of the added volume of toluene and the presence/absence of Fe_3O_4@Ag particles). Thus, the concentration range of DEG for the desired purpose (to obtain electrically conductive micrometric structured elastomer composites) is limited in practice to 15–30% w/w of DEG.

Figure 2 shows optical photographs for some of the first obtained films, with varying filler concentration. The films are disk-shaped with an area, $A \cong 8$ cm^2, slightly smaller than the area of the magnetos used during preparation (although some holes can be observed in Fig. 2 due to the formation of bubbles when evaporating toluene, these regions were cutoff for characterization).

The formation of needles generated by aggregation and alignment of Fe_3O_4@Ag μPs during film preparation can be clearly seen in Figure 3(a). At each point the needles are oriented in the direction of the local magnetic field used during film preparation. Near the center of the film the needles display normal to the surface, while near the edge needles appear mostly in the direction diagonal to the surface. This effect is due to the magnetic field provided by the magnetos during film preparation, which is very uniform in the center but not near the edges. Details of the surface can be observed in the SEM image shown in Figure 3(b).

The needles are formed by grouping Fe_3O_4@Ag μPs. An estimation of the density of needles can be obtained using optical photographs taken with lower magnifications. In films with 4% w/w Fe_3O_4@Ag it was calculated an average density of (14 ± 2) needles mm^{-2} and the needles occupy about 2% of the whole contact area with an average diameter of 42 μm per needle (assuming cylindrical shape). When the amount of particles is increased up to 12% w/w a density of (41 ± 1) needles mm^{-2} was obtained, occupying 11% of the film's area and an average diameter of 58 μm per needle. For films with 25% w/w Fe_3O_4@Ag the formed needles

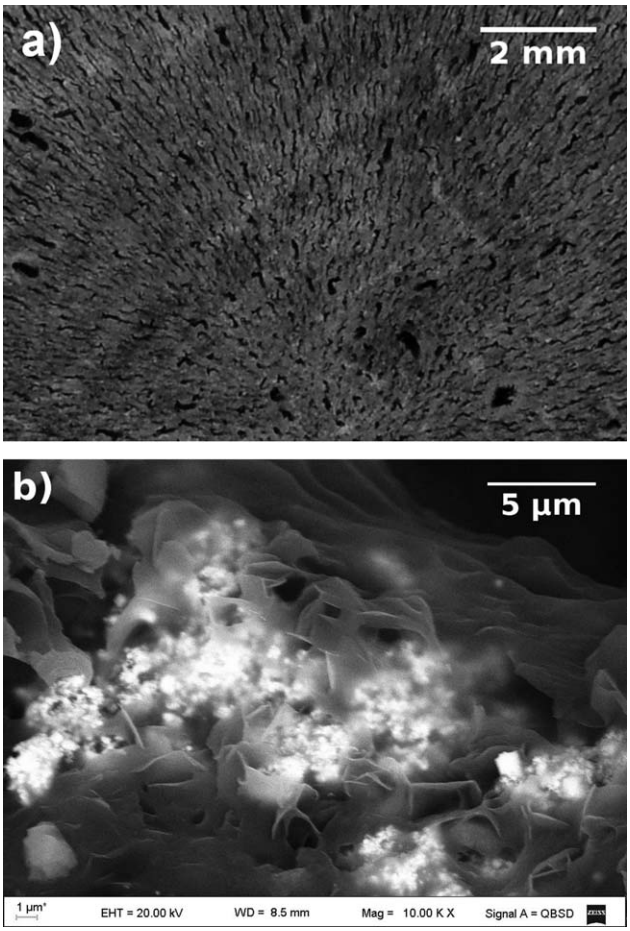

FIGURE 3 SBR-DEG-12% Fe_3O_4@Ag composite films. (a) Optical photograph. (b) SEM image, obtained by electron backscatter detector to emphasize the signal from Fe_3O_4@Ag microparticles.

occupy a large area of the film's surface and it is not easy to discriminate individual needles in order to perform the above calculations with good accuracy.

The thickness of the films, L, as function of the scanned distance was measured using the profilometer described above. Three examples of the recorded profiles are shown in Supporting Information Figure SM2. The average values of L, $<L>$ (calculated as described later) are between (100 ± 10) µm and (150 ± 20) µm varying with the considered film (seven different samples were analyzed). No trend with the scanning rate was observed (12, 20, and 33 µm s^{-1}), nor was a tendency observed between $<L>$ and the composition of the film (e.g., with the proportion of particles). The obtained values of $<L>$ are in very good agreement with observations of the thickness made by SEM using metalized samples (results not shown).

FTIR, DSC, and TGA Analysis of SBR-DEG-Fe_3O_4@Ag Structured Films

The films were analyzed by FTIR spectroscopy (Fig. 4). The SBR spectrum is characterized by the presence of several signals, which appears as bands, peaks, and shoulders, which are described in the following paragraph from higher to lower wavenumbers.

The shoulders at 3060 and 3023 cm^{-1} arise from C—H stretches associated with the $C_{SP}{}^2$—H. The bands centered at 2915 and 2847 cm^{-1} correspond also to C—H stretching of the aliphatic chains in the polymer (with different chemical environments). The signal at 1703–1750 cm^{-1} is attributed to C═O (ν C═O) of carboxylated additives (currently stearic acid and other fatty acids which are added as slippage agents). The peaks observed at 1640 cm^{-1} arise from the C═C modes in the phenyl ring; the bands at 1450 cm^{-1} can be assigned to C═C stretching in the aromatic rings also. The shoulder at 980 cm^{-1} is assigned to the C—H butadiene out-of-plane bending mode, while the band at 964 cm^{-1} to the out-of-plane bending vibrations of the trans —CH═CH— group vibrations of butadiene present in SBR. The band at 910 cm^{-1} is attributed to the out-of-plane bending vibrations of $=CH_2$ of vinyl groups. The strong band at 698 cm^{-1} is attributed to the out-of-plane ring bending mode.

When DEG is added, a broad signal at 3343 cm^{-1} is observed (corresponding to O—H stretching) and two peaks at 1125 and 1055 cm^{-1} appear (attributed to C—O stretching of ether and alcohol groups, respectively). It is interesting to remark that the signal corresponding to carbonyl stretching of the additive is modified in the presence of DEG, an effect that can be assigned to the hydrogen-bond interaction between the hydroxyl groups of DEG and carbonyl groups of the fatty acids.

The addition of µPs produces a shift in the O—H stretching (e.g., from 3343 cm^{-1} in the absence of µPs to 3382 cm^{-1} for 12% w/w Fe_3O_4@Ag). This is considered as an indication of interactions between the Fe_3O_4@Ag µPs and DEG, which increase the strength of the O—H bond producing the observed shift toward higher wavenumbers.

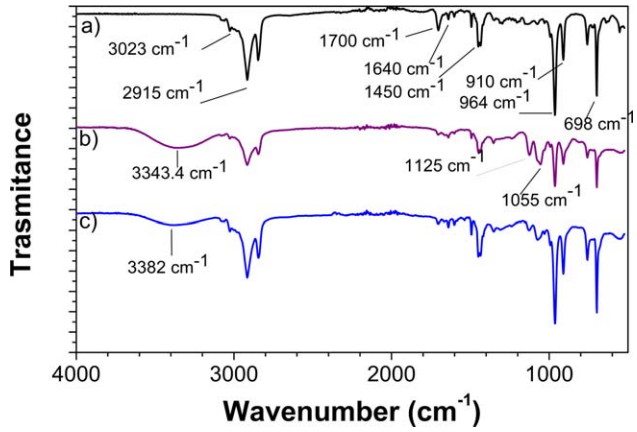

FIGURE 4 FTIR spectra: (a) SBR; (b) SBR-DEG film without µPs; (c) structured composite film SBR-DEG-12% w/w Fe_3O_4@Ag. The percentage of DEG is 18% w/w in (b) and (c). [Color figure can be viewed in the online issue, which is available at wileyonlinelibrary.com.]

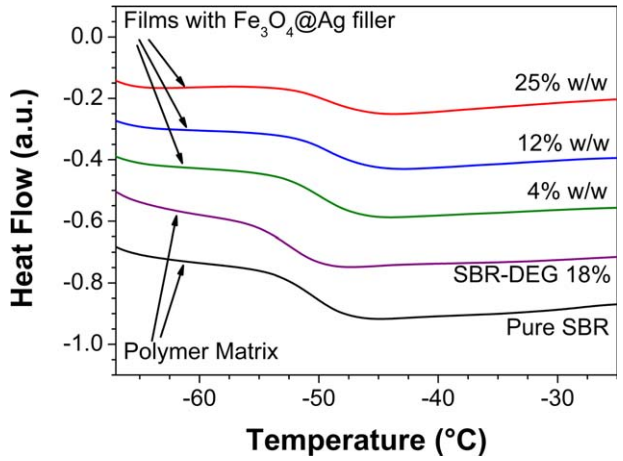

FIGURE 5 DSC thermograms of different matrices (indicated in the figure) including SBR, SBR-DEG, and structured composite films SBR-DEG-Fe_3O_4@Ag, changing the concentration of fillers. The percentage of DEG is 18% w/w in all cases. [Color figure can be viewed in the online issue, which is available at wileyonlinelibrary.com.]

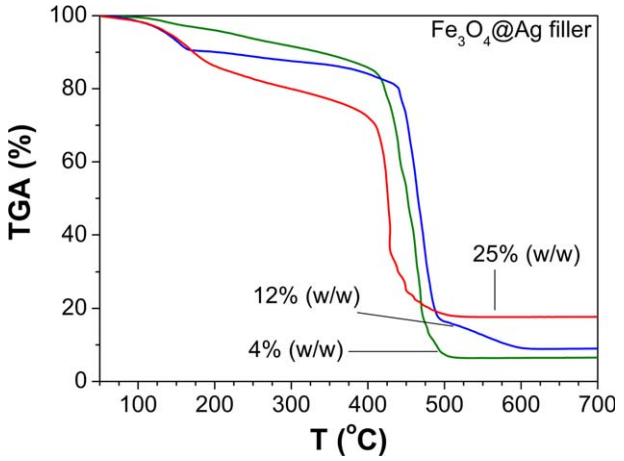

FIGURE 6 TGA thermograms of different SBR-DEG-Fe_3O_4@Ag structured composites, changing the percentage of filler (Fe_3O_4@Ag μPs, indicated in the figure). The percentage of DEG is 18% w/w in all cases. [Color figure can be viewed in the online issue, which is available at wileyonlinelibrary.com.]

The thermal behavior was studied by DSC (see Fig. 5). The values of glass transition temperatures (T_g) for the various composites are shown in Table 1. It is important to note that the $T_g = -50.5$ °C for SBR and the addition of DEG leads to a slight decrease ($T_g = -51.0$ °C for SBR-DEG with 18% w/w of DEG). This fact is due to the plasticizing effect of DEG. However, this behavior is reversed with the μP addition, where the T_g values are higher with the increase in the proportion of μPs in the composites.

The results of TGA are shown in Figure 6. The mass loss in the range 100–200 °C is assigned to evaporation of traces of toluene and water (present in DEG). The losses around 200–250 °C are assigned to evaporation degradation of DEG (boiling point: 245 °C). The loss at 400 °C, under instrumental conditions similar to the present, has been assigned to degradation of SBR.[20] The thermal degradation of SBR is a complex process, in which the most likely pathways have been previously described.[21,22]

Elastic Properties of the SBR-DEG Elastomers

When a normal stress, Σ, is applied and the film thickness, L, decreases, there is a "trivial" effect which contributes to reduce the electrical resistance, R, as $R = L/(\sigma A)$, where A is the area of the film (see Fig. 2 and section "Morphological characterization of SBRDEG-Fe3O4@Ag structured films") and σ the electrical conductance. Hence, it is of central relevance to determine the variation of L with Σ in order to determine the influence of the "trivial" effect on R.

TABLE 1 Glass Transition Temperatures (T_g) Determined by DSC for Different Composites

Sample	T_g (°C)
SBR	−50.5
SBR-DEG[a]	−51.0
SBR-DEG[a]-Fe_3O_4@Ag, 4% w/w[b]	−49.7
SBR-DEG[a]-Fe_3O_4@Ag, 12% w/w[b]	−49.1
SBR-DEG[a]-Fe_3O_4@Ag, 25% w/w[b]	−49.0

[a] The percentage of DEG is 18% w/w.
[b] Percentage of Fe_3O_4@Ag in the composite.

The change of L with Σ was determined by performing stress–strain curves with a texture analysis device (Fig. 7).

As that device allows measuring samples of thickness >1 mm, which avoids measuring stress–strain curves for the structured films, we decide to ensure the quality of the experiments by determining stress–strain curves for thicker samples of the polymer matrix, SBR-18% DEG (and also for pure SBR), in the absence of filler. Therefore, we measured the decrease of the polymer matrix's thickness, L_m, with Σ. Based on our previous results with PDMS-Fe_3O_4@Ag structured samples and in theoretical models, it can be affirmed that the presence of aligned filler particles always produces a hardening of the material.[11,23–25] Hence, the observed decrease of L_m with Σ must be considered as the maximum possible change for the structured films, that is: $L(\Sigma)/L(0) \geq L_m(\Sigma)/L_m(0)$, where $L(0)$ and $L_m(0)$ are the respective values in the absence of applied stress.

Stress–strain cycles of SBR and SBR-18% DEG samples, recorded with a texture analyzer, are shown in Figure 7(a,b), respectively, where samples are compressed at a constant speed (while recording the required force) up to 40% of the initial thickness. Then, when reaching a strain of 40% the compressing probe of the device is completely released and successive compression-release cycles can be performed. It is observed in Figure 7 that reproducible curves are obtained only after at least five stress–strain cycles as, for the latter curves, slightly higher force is required for reaching a 40% strain after each cycle. This effect is more pronounced when

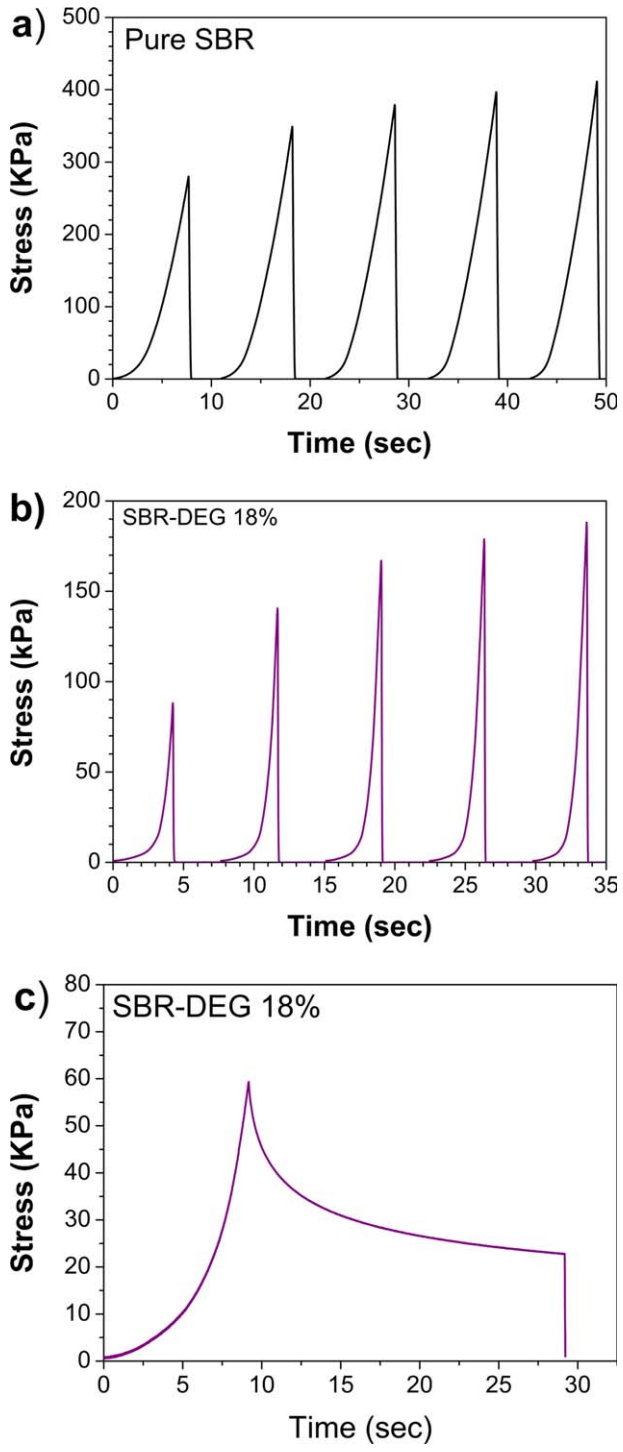

FIGURE 7 Compression stress–strain curves. (a) A sample of SBR is compressed at constant speed up to reaching a 40% strain, followed by a sudden release of compression, then the cycle is repeated. (b) Idem (a) but for a SBR-18% DEG sample. (c) The SBR-18% DEG sample is compressed up to 40% strain, which was kept fixed during 20 s afterward the compressing probe was suddenly released. Speed of compression: 100 μm s^{-1} in the three cases. [Color figure can be viewed in the online issue, which is available at wileyonlinelibrary.com.]

adding DEG [Fig. 7(b)], indicating that at least five compression–decompression cycles must be applied on virgin samples before using them for quantitative determinations of piezoresistive effects. In the case of pure SBR (without adding DEG) it is noted that, after reaching a reproducible regime, the compression stress–strain curves are well fitted by Young's law.

Although the compression stress–strain methodology is not the more appropriated to obtain accurate values of the Young's modulus (because of the relatively limited range of strain, up to 40%) a raw estimation renders a Young's modulus about (0.8 ± 0.1) kPa for the used SBR, in good agreement with a previous estimation of 1 MPa made by our group in a previous work, although calculated using tensile stress–strain curves for SBR of the same styrene:butadiene ratio.[26] On the other hand, the compression stress–strain curves obtained for the SBR-18% DEG matrix are not well described by a single exponent fit (which is the behavior predicted by the Young's law), suggesting a complex relaxation process inside the material whose detailed understanding is beyond the scope of this work, requiring systematic experiments including stress–strain tensile tests.

In addition, Figure 7(c) shows that the polymer matrix (SBR-18% DEG) only reaches relaxation at 30–50 s after applying a stationary strain. Figure 7(c) suggests that this elapsed time is required before registering the magnitude of any physical property when applying a stress on the samples

Concerning the evaluation of the trivial effect, it is concluded from observing and analyzing the curves of Figure 7(b) that when applying a stress $\Sigma = 150$ kPa (maximum value used in piezoresistivity studies) the compression strain is about 22%, thus L_m (150 kPa) $\cong$ 0.78 L_m (0 kPa). Therefore, considering that the strain in the structured films is always less than in the polymer matrix for a given stress, it is concluded that the trivial effect at the maximum applied pressure contributes with less than a 22% at 150 kPa to the total change of R in the structured films. For lower stresses the trivial contribution is even lower. For instance at 80 kPa it is obtained $L_m(80\ \text{kPa})/L_m(0) \cong 0.82$ then $L(80\ \text{kPa})/L(0) > 0.82$ is predicted in the structured film, that is a change less than 18% is the expected contribution of the trivial effect at 80 kPa. These changes cannot explain the variations of R in more than one order of magnitude in the range 0–150 kPa that are described in the next section.

Piezoresistivity of SBR-DEG-Fe_3O_4@Ag Structured Films

Films without DEG do not display significant electrical conductivity (conductivity $<10^{-9}\ \Omega^{-1}\ \text{cm}^{-1}$). That is, no conductance is observed when DEG is absent, even for films with 30% w/w of conductive fillers and/or when they are exposed to relatively high voltages (30 V) and compressing stresses (200 kPa). On the other hand, films with electrical conductivity within our detection limit are obtained when the proportion of DEG is >10% w/w. This suggests that in the absence of DEG (SBR-Fe_3O_4@Ag), the SBR is coating the needles avoiding contact between them and thus the

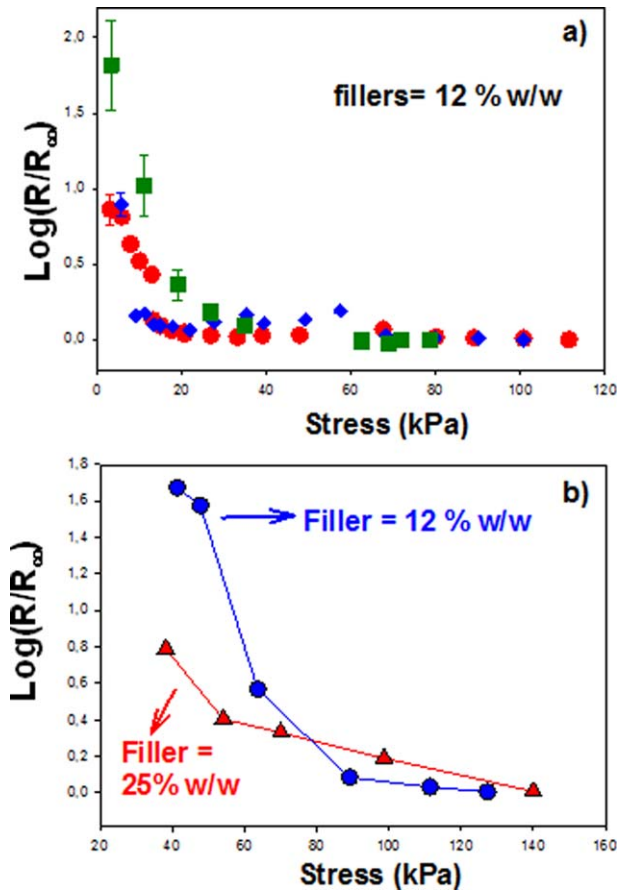

FIGURE 8 Piezoresistivity of SBR-DEG-Fe_3O_4@Ag structured films. *R*, electrical resistance in the direction parallel to the pseudo-chains; R_∞, lowest observed resistance. (a) Test of intra-batch reproducibility and hysteresis for two films ("1" and "2") prepared from the same mixture SBR-DEG-toluene and 12% w/w Fe_3O_4@Ag. (•): Film "1," with stress increased from the lowest value up to 110 kPa. (◆): Film "1" but stress is reduced from 110 kPa to zero in order to test hysteresis. (■): Film "2" with stress monotonously increased. (b) Results for films prepared in another batch where filler concentration was changed (stress was monotonously increased in both cases). Measurements performed in the region where the Ohm's law applies at (25 ± 2) °C. [Color figure can be viewed in the online issue, which is available at wileyonlinelibrary.com.]

electron transport. Electrical conduction in the direction parallel to the needles appears when DEG is added above 10% w/w, indicating that the Fe_3O_4@Ag particles must interact with DEG decreasing the coating of needles by SBR and hence allowing electrical conduction (fillers–DEG interaction was observed in FTIR spectra, see section "FTIR, DSC, and TGA analysis of SBR-DEGFe3O4@ Ag structured films"). No conduction was observed in the direction perpendicular to the needles, that is, the system presents electrical anisotropy as expected in a structured material.

From now on we only refer to *parallel* conduction, that is, when the current flux is in the direction of the needles. Ohmic behavior for conduction in the direction parallel to the needles was verified for applied voltages V_0 below 3–5 V, dependent on the sample (particularly on its thickness) and applied pressures between 3 and 160 kPa. As the thickness of the films is about 100–150 μm, the safe region for the ohmic behavior corresponds to an electric field up to 200 V cm^{-1}.

It is worth to mention that parallel conduction is observed (and measured) when placing metallic contacts at both sides of the films with the condition that both contacts are not laterally displaced (their positions are matched). This reflects the anisotropic characteristic of the material: as there is no conduction in the direction perpendicular to the needles, then the requisite for observing conduction is to match the contacts allowing observing the parallel conduction.

In the ohmic regime, the electrical resistance of the films (always referred to parallel conduction) decreases when a normal compressing stress, Σ, (perpendicular to the area of the films) is applied (Fig. 8). In each determination samples were compressed at the fixed stress for at least 1 min before registering the electrical current. Excellent reproducibility of that response was obtained for samples prepared from a given batch (mixture SBR-DEG-toluene) at a fixed filler concentration without observing hysteresis when performing compression–decompression cycles [Fig. 8(a)] in samples that were previously subjected to stress–strain cycles. The response to a normal stress is reversible, within the experimental error of the determinations [compare data points • and ◆ in Fig. 8(a)].

For samples prepared from a given batch, but changing the amount of filler that is added to the SBR-DEG-toluene mixture, the electrical resistance is higher when the amount of conductive particles is lower, as expected [Fig. 8(a)], excepting variations near saturation.

As described in section "Elastic properties of the SBR-DEG elastomers," the observed changes of *R* cannot be assigned to the trivial effect of decreasing *L* when increasing Σ. Therefore, the results shown in Figure 8 indicate that films present piezoresistivity, that is, variation of σ with Σ. It is reasonable to attribute the piezoresistivity effect to percolation between the conductive needles[24–33] where the percolation probability increases when the films are compressed, in agreement with the increase of σ increases with Σ (decrease of *R* in Fig. 8). In fact, the resistance decreases with Σ to reach a minimum plateau value (saturation of the piezoresistive response). The observation of conductivity in the absence of Σ can be explained by percolation of a given fraction of needles, while saturation of the piezoresistive response at high stresses is in agreement with saturation of percolation between needles.

Magnetoresistance of SBR-DEG-Fe_3O_4@Ag Structured Films

Figure 9 shows the observed increase in the electrical conductivity of the films when a uniform magnetic field, *H*, is applied at a constant stress. As usual, the magnetoresistive

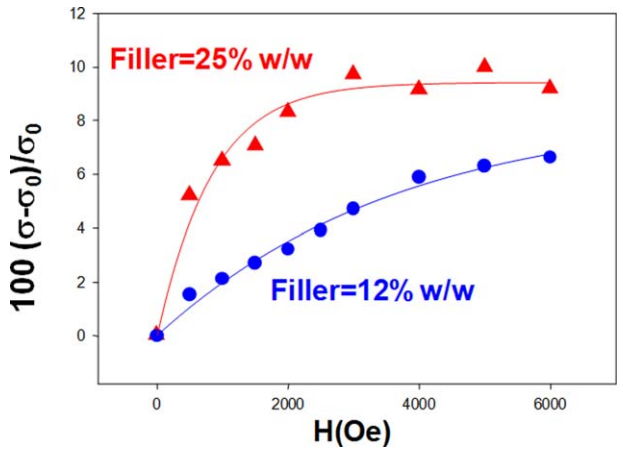

FIGURE 9 Magnetoresistive effect in two SBR-DEG-Fe_3O_4@Ag structured films prepared from the same SBR-DEG-toluene batch, but with different amount of filler particles. σ, electrical conductance in the direction parallel to the pseudo-chains. σ_0, electrical conductance in the absence of magnetic field. *H*, applied uniform magnetic field, monotonously changed from cero. The normal stress is constant, about 40 kPa in both samples. Temperature: (25±2) °C. Filled lines represents fits by exponential growth. [Color figure can be viewed in the online issue, which is available at wileyonlinelibrary.com.]

effect is presented as the percentage change of the electrical conductivity.

The magnetic field is applied in the direction parallel to the electrical flux and to the stress, that is, perpendicular to the surface of the film. A normal stress ($\Sigma = 40$ kPa) was applied on the samples. The electrical resistances are in the order of 1–10 Ω, being lower for the films with larger amount of fillers.

The observed changes are similar or larger than those currently reported for magnetoresistance effects in solid-state systems formed by juxtaposition of magnetic–conductive layers. For instance, Péter et al. reported a 6% change using Co–Cu/Cu multilayer system with superparamagnetic regions on a silicon wafer.[34] Nevertheless, the magnitude of the magnetoresistive effect presented here is lower than that observed in our group for structured dispersions of superparamagnetic fillers in PDMS (e.g., 50% at 1.5 kOe) and also for systems reported by other groups using conductive and nonconductive polymer matrices.[11,35–45] In the case of PANI and epoxy nonstructured matrices using superparamagnetic Fe_3O_4 as fillers,[35,36] large and giant magnetoresistance effects have been reported, and the origin of magnetoresistance effects in those disordered systems was assigned to quantum effects, including variable range hopping (VRH) processes.[37,38] However, it is not straightforward to compare different reports as several aspects must be considered, such as distinguishing between viscous fluid and elastic-nonfluid systems, structured and nonstructured, thick slices (millimeters) or submillimeter films, superparamagnetic of ferro-ferri magnetic samples, the applied stress on the sample, and so forth. There are actually many reports in literature presenting different systems displaying magnetoresistance effects in rheological structured composites (always showing increase of the electrical conduction with the magnetic field, as far as we know). Some examples are described here below. Recently, Bica et al. reported an 18% increase in the conductivity when applying about 1 kOe although in a nonstructured and nonelastic but viscous system (silicon oil with carbonyl iron linked to graphene as fillers).[39] Also in a recent article, Ausanio et al. reported about 100% of magnetoresistance, but when applying nonuniform magnetic fields in nonstructured and 2 cm thickness samples with iron particles (or nickel) dispersed in silicone.[40,41] Kchit et al.[42] reported giant magnetoresistive effects for structured dispersions of nickel in silicone, which is probably the largest magnetoresistive effect reported in rheological systems (changes of several orders of magnitude when applying 2 kOe), although in 2 mm samples and in a polymer with relatively low Young's modulus (200 kPa). It is worth mentioning that in the case of using intrinsic conductive polymers (e.g., PANI) the physical process involved in the magnetoresistance process is completely different and it has been recently reviewed for polyaniline-based systems.[42,46]

In the present case (and also in our previous work), the magnitude of the magnetoresistive effect is dependent on the filler concentration: 9% for 25% w/w and 6% for 12% w/w.[11] Data points of Figure 9 are empirically fitted by exponential growth: $100\left(\frac{\sigma-\sigma_0}{\sigma_0}\right)=A_\infty(1-\exp(-H/H_1)$, recovering $A_\infty = (9.4 \pm 0.3)$ and (8.5 ± 0.7) for 25 and 12% filler, respectively; $H_1 = (0.83 \pm 0.07)$ kOe and (3.7 ± 0.5) kOe for 25 and 12% filler, respectively. The system seems to reach saturation of the magnetoresistive response with *H*, although the characteristic field required for saturation, provided by H_1, is larger in the case of the lowest amount of filler particles. The increase of electrical conduction in piezo or magneto resistive effects observed in structured percolating rheological materials have been assigned to an increase of the number of electrical contacts between the conductive fillers (in our case, the pseudo-chains (needles) formed during preparation) when an external stimulus, stress, or magnetic field is applied (spin effects on the electron scattering are neglected).[39–45] Thus, the origin of the observed changes, both in the case of piezoresistivity and magnetoresistivity, is generally assigned to the increase of percolation, as described in Section "Piezoresistivity of SBR-DEG- Fe3O4@Ag structured films." However, in the case of magnetoresistivity, it seems that a comprehensive theory, which should quantitatively include how the percolation probability and tunnel effects between pseudo-chains increase when applying a magnetic field, is not yet developed. Thus, the fits and recovered parameters presented here must be considered for comparison purposes only. The larger value of H_1 obtained for the films with lower amount of fillers can be rationalized if assuming that when there is less density of needless there is less density of electrical contacts and therefore larger magnetic fields are required in order to increase the percentage of those contacts and thus increase the conduction. Further elaborations are beyond the scope of this work.

CONCLUSIONS

The systems studied in this work are composites formed by dispersions of conductive and magnetic particles dispersed in a nonconductive elastomer polymer. The fact that the polymer matrix is an insulator classify these systems in a very different group with respect to those formed by conductive polymers, typically polyaniline, where conduction is given by the matrix itself. This generates different types of opportunities and drawbacks for applications in electronic components, magnetoelectric devices, flexible electronics, and so forth. For example, as the condition of having a conductive polymer as the matrix is no longer required, then it is possible to extend the range of possible different polymers with the opportunity to optimize the choice of different matrices depending on the desired applications. As an example, the systems based on SBR and PDMS have different elastic–mechanic properties but both can be used as piezo and/or magneto resistive materials. However, the fact that the matrix is essentially an insulator implies the need to add conductive particles in excess of a critical value above which appreciable conductivity appears (conductivity higher than the conductivity of the matrix, displaying ohmic behavior and electrically reversible). Depending on the chemical nature and morphology of the particles used (and the chosen matrix), the critical concentrations can be very different, including relatively high values (e.g., 50% w/w in the case of PDMS graphite platelets).[47,48] This implies some difficulties and disadvantages. For example, an important factor to consider is the increased costs of both labor and materials synthesis in the case of using *ad hoc* synthesized nanomaterials. Another difficulty is that the use of high levels of filler particles induces significant changes in the elastic properties of the composite with respect to the polymeric matrix, distorting the advantages offered by the possibility of choosing the polymer. These difficulties are circumvented by the use of structured systems as those presented in this work. Recently, we performed Monte Carlo simulations of two-dimensional stick systems with anisotropic alignments, finding that there is a wide and well-defined range of values for the standard deviation of the angular distribution for which it is possible to obtain reliable anisotropic percolation under experimental conditions similar to those presented here.[49]

Thus, to use magnetic particles as fillers allows generating a defined anisotropic structure in the films given by the formation of oriented pseudo-chains (needles) of inorganic material inside the polymer matrix. The fact that they are also electrically conductive films provides the piezoresistive and magneto resistive properties. The formation of pseudo-chains aligned in a specific direction reduces the critical concentration for observing electrical conduction (which is between 4 and 12% w/w in this work) or it increases the sensitivity of the conductance with the external pressure.[9,28,50]

In addition, the formation of aligned pseudo-chains induces anisotropic properties in the material. In previous works, where we have used other filler particles (nickel NPs and nanochains, cobalt-ferrites NPs) and anisotropic properties, such as elasticity, magnetization curves, and magnetic resonances were detected and described for composites with proportions between 2 and 15% w/w of filler particles, although not in films but in millimeter slides using PDMS as matrix.[11–14] In the case of the SBR-DEG-Fe_3O_4@Ag systems presented in this work, the following was observed concerning electrical anisotropic properties of the films: (a) transverse electrical conduction through the main faces of the films (parallel to the direction of the aligned pseudo-chains) is only obtained when electrical contacts are facing exactly on both sides of the films; (b) no conduction in the direction perpendicular to the pseudo-chains was detected, for example, not on the surface of the films nor when placing contacts at the side edges. This anisotropic behavior is of central importance to the application of the films in electronic components based on polymeric materials. In summary, the structure induced in the material is the first aspect on which to remark, because it decreases the percolation critical point to observe conductivity and induces anisotropic properties in the material. Thus, the physical properties of structured systems are different than random filler–matrix composites including those where the fillers are synthesized within the polymer using *in situ* procedures.[51,52]

The second key factor presented in this work in the case of films based on SBR submillimeter films is the addition of DEG which prevents formation of a bound rubber layer on the pseudo-chains (a phenomenon recently described in the case of multiwall carbon nanotubes dispersed in SBR, which avoids percolation and thus conduction).[53] The addition of DEG in percentage higher than 10% is required for the films of SBR-DEG particles to present measurable electrical conductivity in the direction parallel to the pseudo-chains. Moreover, addition of DEG avoids the need for other treatments of the material, such as swelling by solvent vapors (which was tested without success in the present case) or functionalizing the inorganic fillers. Thus, by using SBR loaded with DEG it was not necessary to make any mechanical or chemical surface treatments to have electrical conduction from one side to the other of the films. The preparation procedure, based on the slow evaporation of the solvent in the presence of magnets located above and below a defined volume of the system, allows obtaining homogeneous and structured films of about 100 μm thick with low dispersion in thickness. Although including DEG generates significant changes in the elastic matrix, the final material has no significant irreversible effects in its piezo and magneto resistive responses. Thus, the generation of elastic films with the described properties is a significant advance for its application in flexible electronics and in the areas of electronic devices and polymer-based components.

ACKNOWLEDGMENTS

GJ, ND, and RMN are research members of the National Council of Research and Technology (CONICET, Argentina). MMR is a PhD student at the University of Buenos Aires (UBA) with a

doctoral fellowship from CONICET. Financial support was received from UBA (UBACyT 2012-2015, projects 2002 01101 00098 and 2002 201001 00142), CONICET (PIP 112-201101-00370CO), and Ministry of Science, Technology and Innovations (MINCYT- FONCYT, Argentina, PICT 2011-0377 and PICT-2012-0717). The authors thank Angel Marzocca (FATE S.A.I.C., Argentina) for providing the SBR and the *Laboratorio de Bajas Temperaturas* (School of Sciences, UBA) for facilities concerning magnetic measurements. The Center of Documental Production (CePro) and the Center of Advanced Microscopy (CMA), School of Sciences, University of Buenos Aires, are acknowledged for obtaining the presented pictures and SEM-TEM images. Industrial Designer Luciana Feo Mourelle is acknowledge for designing the graphical abstract.

REFERENCES AND NOTES

1 G. V. Stepanov, S. S. Abramchuk, D. A. Grishin, L. V. Nikitin, E. Y. Kramarenko, A. R. Khokhlov, *Polymer* **2007**, *48*, 488–495.

2 Z. Varga, G. Filipcsei, M. Zrínyi, *Polymer* **2006**, *47*, 227–233.

3 D. Ivaneyko, V. P. Toshchevikov, M. Saphiannikova, G. Heinrich, *Macromol. Theory Simul.* **2011**, *20*, 411–424.

4 K. Shahrivar, J. de Vicente, *Soft Matter* **2013**, *9*, 11451–11456.

5 K. Danas, S. V. Kankanala, N. Triantafyllidis, *J. Mech. Phys. Solids* **2012**, *60*, 120–138.

6 I. Bica, Y. D. Liu, H. J. Choi, *Colloid Polym. Sci.* **2012**, *290*, 1115–1122.

7 J. L. Mietta, G. E. Jorge, R. M. Negri, *Smart Mater. Struct.* **2014**, *23*, 85026–85038.

8 W. H. Li, X. Z. Zhang, H. Du, Magnetorheological Elastomers and Their Applications, Advances in Elastomers I; Springer: Berlin/Heidelberg, **2013**; pp 357–374.

9 N. Kchit, G. Bossis, *J. Phys. Condens. Matter* **2008**, *20*, 204136–204141.

10 J. L. Mietta, G. E. Jorge, O. E. Perez, T. Maeder, R. M. Negri, *Sens. Actuators A: Phys.* **2013**, *192*, 34–41.

11 J. L. Mietta, M. M. Ruiz, P. S. Antonel, O. E. Perez, A. Butera, G. E. Jorge, R. M. Negri, *Langmuir* **2012**, *28*, 6985–6996.

12 R. A. Landa, P. S. Antonel, M. M. Ruiz, O. E. Perez, A. Butera, G. Jorge, C. L. P. Oliveira, R. M. Negri, *J. Appl. Phys.* **2013**, *114*, 213912–213923.

13 A. Butera, N. Alvarez, G. Jorge, M. M. Ruiz, J. L. Mietta, R. M. Negri, *Phys. Rev. B.* **2012**, *86*, 144424–144432.

14 P. S. Antonel, G. Jorge, O. E. Perez, A. Butera, G. Leyva, R. M. Negri, *J. Appl. Phys.* **2011**, *110*, 43920–43921.

15 M. M. Nobrega, J. Bonametti Olivato, A. P. Bilck, M. V. Eiras Grossmann, F. Yamashita, *Mater. Sci. Eng. C.* **2012**, *32*, 2220–2222.

16 M. C. Goldner, O. E. Pérez, A. M. R. Pilosof, M. Armada, *LWT Food Sci. Technol.* **2012**, *4*, 83–90.

17 R. Valenzuela, M. C. Fuentes, C. Parra, J. Baeza, N. Duran, S. K. Sharma, M. Knobel, J. Freer, *J. Alloys Compd.* **2009**, *488*, 227–231.

18 M. Knobel, W. C. Nunes, L. M. Socolovsky, E. De Biasi, J. M. Vargas, J. C. Denardin, *J. Nanosci. Nanotechnol.* **2008**, *8*, 2836–2857.

19 V. L. Kirillov, D. A. Balaev, S. V. Semenov, K. A. Shaikhutdinov, O. N. Martyanov, *Mater. Chem. Phys.* **2014**, *145*, 75–81.

20 K. Xiang, X. Wang, G. Huang, J. Zheng, J. Huang, G. Li, *J. Therm. Anal. Calorim.* **2014**, *115*, 247–254.

21 M. J. Fernández-Berridi, N. Gonzalez, A. Mugica, C. Bernicot, *Thermochim. Acta* **2006**, *444*, 65–70.

22 K. Xiang, X. Wang, G. Huang, J. Zheng, J. Huang, G. Li, *Polym. Degrad. Stab.* **2012**, *971*, 704–1715.

23 Y.-P. Wu, Q.-X. Jia, D.-S. Yu, L.-Q. Zhang, *Polym. Test.* **2004**, *23*, 903–909.

24 E. Coquelle, G. Bossis, D. Szabo, F. J. Giulieri, *Mater. Sci.* **2006**, *41*, 5941–5953.

25 C. Y. Hui, D. Shia, *Polym. Eng. Sci.* **1998**, *38*, 774–782.

26 A. De Falco, M. Lamanna, S. Goyanes, N. B. D'Accorso, M. L. Fascio, *Physica B* **2012**, *407*, 3175–3177.

27 J. Ho Kang, C. Park, J. A. Scholl, A. H. Brazin, N. M. Holloway, J. W. High, S. E. Lowther, J. S. Harrison, *J. Polym. Sci., Part B: Polym. Phys.* **2009**, *47*, 994–1003.

28 D. Wu, L. Wu, F. Gao, M. Zhang, C. Yan, W. Zhou, *J. Polym. Sci., Part B: Polym. Phys.* **2008**, *46*, 233–243.

29 G. Ambrosetti, C. Grimaldi, I. Balberg, T. Maeder, A. Danani, P. Ryser, *Phys. Rev. B* **2010**, *81*, 155434–155446.

30 B. Nigro, C. Grimaldi, P. Ryser, A. P. Chatterjee, P. van der Schoot, *Phys. Rev. Lett.* **2013**, *110*, 015701.

31 I. Balberg, *J. Phys. D: Appl. Phys.* **2009**, *42*, 064003–064011.

32 J. Krückel, D. W. Schubert, *Eur. Polym. J.* **2014**, *53*, 50–57.

33 A. Sarvi, U. Sundararaj, *Synth. Met.* **2014**, *194*, 109–117.

34 L. Péter, V. Weihnacht, J. Tóth, J. Pádár, L. Pogány, C. M. Schneider, I. Bakonyi, *J. Magn. Magn. Mater.* **2007**, *312*, 258–265.

35 H. Gu, Y. Huang, X. Zhang, Q. Wang, J. Zhu, L. Shao, N. Haldolaarachchige, D. P. Young, S. Wei, Z. Guo, *Polymer* **2012**, *53*, 801–809.

36 H. Gu, S. Tadakamalla, Y. Huang, H. A. Colorado, Z. Luo, N. Haldolaarachchige, D. P. Young, S. Wei, Z. Guo, *App. Mat. Interfaces.* **2012**, *4*, 5613–562.

37 H. Gu, J. Guo, X. Zhang, Q. He, Y. Huang, H. A. Colorado, N. Haldolaarachchige, H. Xin, D. P. Young, S. Wei, Z. Guo, *Chem. Soc. Rev.* **2013**, *42*, 5907–5943.

38 H. Gu, X. Zhang, H. Wei, Y. Huang, S. Wei, Z. Guo, *J. Phys. Chem. C* **2013**, *117*, 6426–6436.

39 I. Bica, E. M. Anitas, M. Bunoiu, B. Vatzulik, I. Juganaru, *J. Ind. Eng. Chem.* **2014**, *20*, 3994–3999.

40 G. Ausanio, C. L Hison, V. Iannotti, L. Lanotte, L. Lanotte, *J. Appl. Phys.* **2011**, *110*, 063903–063903.

41 G. Ausanio, V. Iannottia, E. Ricciardi, L. Lanotte, L. Lanotte, *Sens. Actuators A: Phys.* **2014**, *205*, 235–239.

42 N. Kchit, P. Lancon, G. Bossis, *J. Phys. D: Appl. Phys.* **2009**, *42*, 105506–105510.

43 A. Stoll, M. Mayer, G. J. Monkman, M. Shamonin, *J. Appl. Polym. Sci.* **2014**, *131*, 39793–39799.

44 X. Qiao, X. Lu, W. Li, J. Chen, X. Gong, T. Yang, W. Li, K. Sun, X. Chen, *Smart Mater. Struct.* **2012**, *21*, 115028.

45 J. E. Martin, R. A. Anderson, J. Odinek, D. Adolf, J. Williamson, *Phys. Rev. B.* **2003**, *67*, 094207–094217.

46 H. Gu, J. Guo, X. Yan, H. Wei, X. Zhang, J. Liu, Y. Huang, S. Wei, Z. Guo, *Polymer* **2014**, *55*, 4405–4419.

47 A. Celzard, E. McRae, C. Deleuze, M. Dufort, G. Furdin, J. F. Maréché, *Phys. Rev. B* **1996**, *53*, 6209–6214.

48 R. M. Negri, S. D. Rodriguez, D. L. Bernik, F. V. Molina, A. Pilosof, O. E. Pérez, *J. Appl. Phys.* **2010**, *107*, 113703–113714.

49 J. L. Mietta, R. M. Negri, P. I. Tamborenea, *J. Phys. Chem. C* **2014**, *118*, 20594–20604.

50 J. L. Mietta, University of Buenos Aires, Personal communication, August 2014.

51 G. S. Rajan, K. A. Mauritz, S. L. Stromeyer, T. Kwee, P. Mani, J. L. Weston, D. E. Nikles, M. Shamsuzzoha, *J. Polym. Sci., Part B: Polym. Phys.* **2005**, *43*, 1475–1485.

52 M. Chipara, I. Morjan, R. Alexandrescu, J. M. Zaleski, N. Remmes, D. V. Baxter, *J. Polym. Sci., Part B: Polym. Phys.* **2005**, *43*, 3432–3437.

53 S. K. Peddini, C. P. Bosnyak, N. M. Henderson, C. J. Ellison, D. R. Paul, *Polymer* **2014**, *55*, 258–270.